Conditions at interfaces of layered flow with intense bed load transport

Václav Matoušek[1,*], *Jan* Krupička[1], *Tomáš* Picek[1], *Štěpán* Zrostlík[1]

[1]Czech Technical University in Prague, Faculty of Civil Engineering, 166 29 Prague 6, Czech Republic

Abstract. Intense bed load transport in open channel flow is typically associated with a layered structure of the flow, in which individual layers exhibit different mechanisms of support and friction of transported sediment grains. In the lowermost layer adjacent to the channel bed, the grains slide over each other and maintain virtually permanent contact. In the uppermost layer below the water surface, typically no grains are transported. In the central layer, the grains collide with each other producing typical distributions of granular concentration and velocity across the collisional layer. Mathematical models describing the layered flow with intense bed load (as models based on kinetic theory of granular flows) consider flow conditions at interfaces of the individual layers in their flow predictions. Usually, experimental verification of interfacial predictions is lacking. We exploit results of our new experiments with plastic cylindrical sediment to identify a variation of the conditions at the interfaces (local interfacial granular concentrations and velocities) with varying flow discharge, depth and slope in a laboratory tilting flume. The experimental results include local granular concentration using an improved laser stripe method. The experiments are compared with predictions using our kinetic-theory based transport model with the aim to evaluate a match for experimentally-determined and model-predicted interfacial parameters.

1 Introduction

Flash flood events on steep-slope mountain channels or transient flows e.g. due to dam break lead to vast masses of sediment transported through a channel with a mobile bed. Usually, the sediment is transported in intense bed load regime in which collisional interactions dominate as mechanisms of grain support and flow resistance in the channel. It is poorly understood how to describe the governing mechanisms that interrelate key flow parameters in such flows. So far, collisional mechanisms are poorly understood and hence modelling approaches are seldom sufficiently accurate.

Typically, high concentrated sediment laden flows tend to exhibit a layered structure in which a vast majority of grains is transported through a collisional transport layer. The kinetic theory of granular flows is an appropriate approach to modelling of flows dominated by granular collision. Kinetic-theory based models for contact-load transport in open-channel flow enable a prediction of relevant flow quantities in a layered pattern of the flow [1-4]. The existing models differ mainly in assumptions taken to calculate granular flows under particular studied conditions, some including mechanism of turbulent suspension supporting part of transported grains [5].

In this paper, we use our recently formulated simple model based on classical kinetic theory [6] to evaluate flow conditions observed in our intense-bed-load experiment of a new particulate sediment fraction in our laboratory tilting flume.

2 Experimental work

Results are presented of tilting-flume experiments carried out in the Water Engineering Laboratory of Czech Technical University in Prague during 2018. A new granular material was tested. The experimental procedure was the same as for the earlier tests with other granular fractions [7] although an important extension of the measurement was reached by implementing one new measuring technique. Our experiments included measurements of distribution of granular concentration across the flow depth.

2.1 Flow conditions

We investigate steady uniform turbulent open-channel flow of mixture of water and solid particles over mobile bed in the upper-stage plane bed regime. Due to grain properties and flow conditions, it is assumed that the transported grains are supported exclusively by mutual contacts (primarily collisions) and their turbulent suspension is negligible.

Typically, our measuring campaigns include tests for different discharges and a broad range of delivered volumetric concentrations of tested sediment.

* Corresponding author: v.matousek@fsv.cvut.cz

The new experiments were carried out with plastic PVC particles (fraction code FA60) of a cylindrical shape (Figure 1) and the mass-median diameter of equivalent sphere 6.42 mm, the density 1411 kg/m^3, and the terminal settling velocity 0.179 m/s. The properties are summarized in Table 1, in which they are also compared with a similar granular material (fraction code TLT50) tested earlier.

Table 1. Properties of experimental bed-load particles

Properties	FA60	TLT50
h_p*(mm)*	4.97	4.90
d_c(mm)	6.11	4.75
d_e (mm)	6.42	5.41
v_t (m.s^{-1})	0.179	0.149
ρ_s (kg . m^{-3})	1411	1307

h_p – average height of cylinder, d_c – average diameter of cylinder, d_e – diameter of equivalent sphere adequate to d_{50}, v_t – terminal settling velocity, ρ_s – grain density

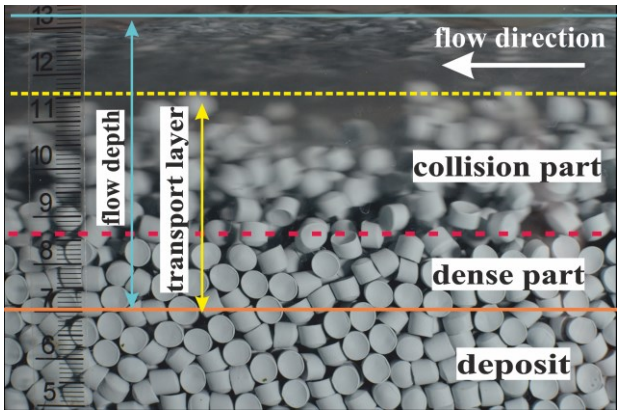

Fig. 1. Layered flow condition in flow transporting the FA60 plastic grains.

Figure 1 shows a typical structure of the observed particle-laden flow in the upper-plane bed regime. The flow is layered with a water layer below the water surface and the transport layer sub-divided to the upper collisional part and the lower dense sliding part just above the plane top of the stationary deposit. The thickness of the individual layers varies with the bed shear stress and the collisional region tends to dominate at high bed shear. This typical layered character of the flow has been observed in our earlier tests with other sediments as well and it is described in detail for instance in [8].

2.2 Experimental set up and measurement techniques

2.2.1 Tilting flume

The experiment was carried out in our recirculating tilting flume with a rectangular cross section. It is 8 m long, 0.20 m wide, and 0.27 m deep. Positions of flow interfaces (water surface, positions of individual layers) are measured in 5 cross sections along the flume. The flume and its measuring equipment (magnetic flowmeter, differential pressure transducers, water surface acoustic sensors, flume inclination meter etc.) are described elsewhere [9].

2.2.2 Measuring techniques

A distribution of local velocity across the flow depth is measured by two independent measuring techniques - Prandtl tube and Ultrasonic Velocity Profiler [7]. The new measurement of a distribution of local volumetric concentration of grains across the transport layer is carried out using the camera-based laser stripe method [10-11]. The measuring equipment is composed of a camera and a laser source.

For the FA60 tests, we used a diode source of green laser sheet (Blau Optoelektronik FP-Mvnano-520-30-30-F, 30 mW, 520 nm) and a sequence of sensed photos was recorded by the high speed camera Dantec Dynamics FlowSense EO 4M-41 with the objective Carl Zeiss Planar 1.4/50 ZF. Resolution of photos was set to 1768 x 2352 pixels and image frequency was 58 fps. We used aperture f/16.

2.2 Experimental results

We carried out 18 experiments with FA60 of which 13 included measured velocity and concentration profiles (discharge either 8 l/s or 10 l/s approximately). The remaining 5 measurements were carried out for other discharges corresponding with the upper or lower thresholds of the upper plane bed regime. Ranges of measured integral parameters of flow are summarized for the FA60-test and compared with similar earlier TLT50-tests in Table 2.

Table 2. Range of integral quantities of flow in experiments.

Material	FA60		TLT50	
Number of test runs	18		55	
Quantity	min	max	min	max
Flow velocity (m/s)	0.62	0.90	0.30	1.04
Flow depth (mm)	53	77	47	101
Bed slope (-)	0.012	0.079	0.003	0.054
Delivered concentration (-)	0.013	0.308	0.010	0.294
Shields parameter (-)	0.28	2.23	0.27	2.06
Froude number (-)	0.77	1.06	0.76	1.33

Figure 2 shows the thickness of the dense part of the transport layer detected from observations of the video records. It demonstrates that the dense part of the transport layer develops only if the dimensionless bed shear stress (bed Shields parameter) exceeds approximately one. This is consistent with our previous tests with other plastic sediment fractions.

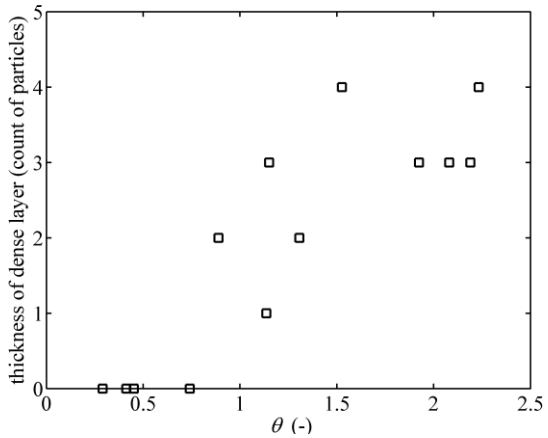

Fig. 2. Observed thickness of dense part of transport layer counted as multiple of grain size related to measured dimensionless bed shear stress (bed Shields parameter)

2.3.1 Distribution of velocity

In Figures 3 to 5, measured distributions of local velocity across the flow depth are plotted as black x-signs. Consistent with the previous tests, the measured shapes of the profiles can be considered across the collisional part of the transport layer provided that the layer is sufficiently thick in comparison with the flow depth (Figures 4 and 5). In the water layer above the transport layer, the velocity profile tends to be logarithmic, again provided that the water layer is sufficiently thick (e.g. Figure 3).

If the dense part of the transport develops at high bed shear (Figures 4 and 5) then the linear profile of the collisional layer is linked to the almost uniform profile across the dense layer. Velocity of grains sliding in the dense layer tends to be significantly lower than the local velocity of grains in the core of the collisional layer.

2.3.2 Distribution of concentration of grains

The measured distributions of the volumetric concentration of grains for flows of different bed shear stress are plotted in Figures 3 to 5 as red squares. The local concentration increases with the depth within the collisional part of the transport layer, being zero at the top of the layer and reaching maximum value at the bottom of the collisional layer. The maximum concentration reaches a value very similar to the bed concentration in the deposit if the Shields parameter is very high (Figure 5), while the maximum value at the bottom of the collisional layer tends to be lower than the bed concentration if the Shields is low (significantly lower in Figure 3, slightly lower in Figure 4). The difference between the local concentration at the bottom of the collisional layer and in the deposit seems to be very sensitive to a value of the Shields parameter. This measurement-based observation confirms results of our analysis based on the earlier experiments without measured concentration profiles [8]. The observation is important for layered-flow based modelling of intense bed transport. Present models do not take this effect into account and assume that the local concentration at the bottom of the collisional layer is the same as the bed concentration.

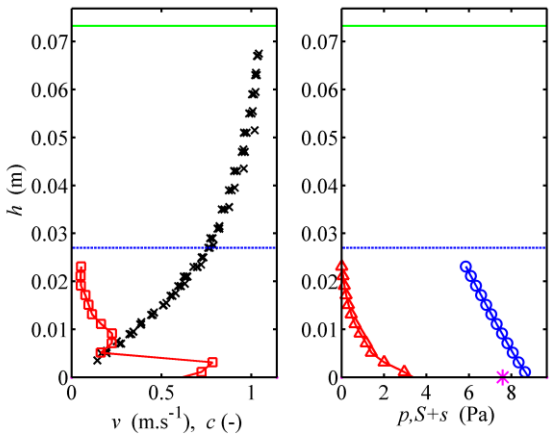

Fig. 3. Distributions in layered flow of FA60-mixture (bed Shields parameter = 0.2). Left plot - measured distribution of volumetric concentration and velocity. Right plot – calculated solids normal stress and total shear stress. Legend: black x – velocity profile, red square – concentration profile, from top to bottom: green line - water surface, blue line – top of transport layer, magenta line - top of dense layer; right plot: red triangle – normal stress, blue circle - total shear stress, magenta star – bed shear stress computed from measured integral data

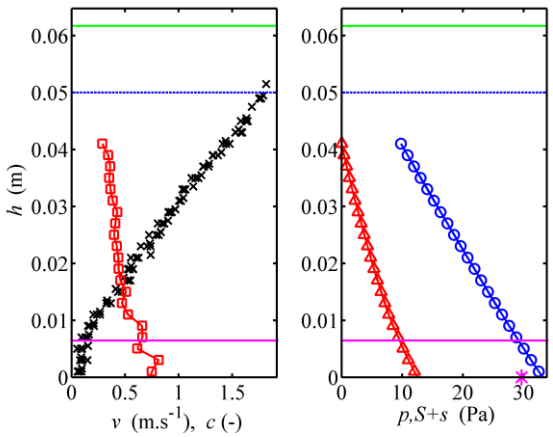

Fig. 4. Distributions in layered flow of FA60-mixture (bed Shields parameter = 1.1). Left plot - measured distribution of volumetric concentration and velocity. Right plot – calculated solids normal stress and total shear stress. Legend: black x – velocity profile, red square – concentration profile, from top to bottom: green line - water surface, blue line – top of transport layer, magenta line - top of dense layer; right plot: red triangle – normal stress, blue circle - total shear stress, magenta star – bed shear stress computed from measured integral data

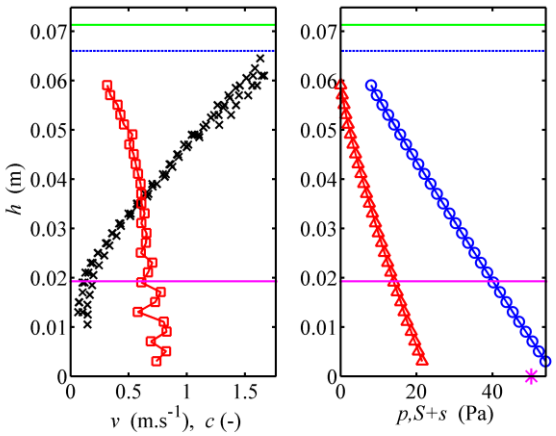

Fig. 5. Distributions in layered flow of FA60-mixture (bed Shields parameter = 1.9). Left plot - measured distribution of volumetric concentration and velocity. Right plot – calculated solids normal stress and total shear stress. Legend: black x – velocity profile, red square – concentration profile, from top to bottom: green line - water surface, blue line – top of transport layer, magenta line - top of dense layer; right plot: red triangle – normal stress, blue circle - total shear stress, magenta star – bed shear stress computed from measured integral data

3 Analysis and discussion

3.1. Distribution of granular stresses

The measured distribution of local concentration can be employed to determine the distributions of the grain-related stresses across the transport layer of sediment-laden flow using equations based on the principle of momentum balance. The local granular normal stress p balances the normal component of the submerged weight of grains,

$$p = \left(\rho_s - \rho_f\right) \cdot g \cdot \cos\omega \cdot \int_0^H c \cdot dh \qquad (1)$$

where ρ_f is density of fluid, g is gravity acceleration, ω is slope of flow and c is volumetric concentration. The total shear stress composed of the granular component s and fluid component S is related to the longitudinal component of the weight of the mixture burden above the local position h,

$$S + s = g \cdot \sin\omega \cdot \int_0^H \left[\rho_s \cdot c + \rho_f \left(1 - c\right)\right] \cdot dh \qquad (2)$$

Distributions of the stresses calculated from the measured distributions of concentrations using Equations 1 and 2 are given in the right plots of Figures 3 to 5. The distributions provide also values of stress at the flow interfaces.

The total shear stress at the top of the deposit (the bed shear stress) obtained from the distribution using Equation 2 is compared with the bed-width averaged shear stress calculated from the integral quantities of the flow (including the side-wall effect) in Figures 3 to 5. The agreement is good although the width-averaged bed stress tends to be slightly lower than the stress from the concentration distribution. The local distribution-derived stresses at another interface, namely at the bottom of collisional part of transport layer, are plotted in Figure 6. Unsurprisingly, they exhibit a close correlation with the bed Shields parameter (the dimensionless width-averaged total bed shear stress).

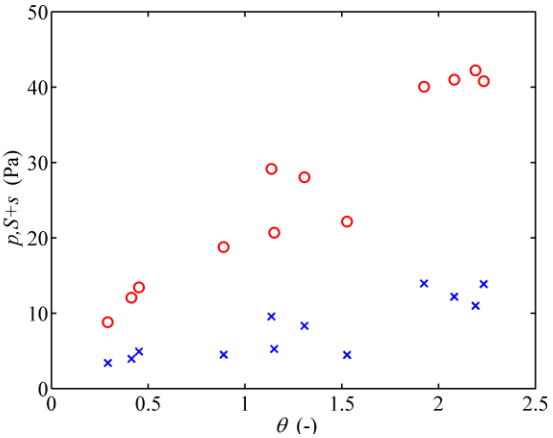

Fig. 6. Local normal granular stress and total shear stress at bottom of collisional part of transport layer related to bed Shields parameter. Legend: circle – total shear stress, cross – normal granular stress.

3.2 Comparison of flow integral parameters of FA60-mixture and TLT50-mixture

Besides local values of flow quantities, it is also interesting to analyse integral (cross-section averaged) quantities of the sediment-laden flow. In order to broaden a perspective of the analysis, we compare integral-quantity results for the FA60-flow with the results of similar TLT50-flow tested in our tilting flume earlier. The shape of FA60-particles and TLT50-particles is virtually the same, the density and size are different for the two fractions (see Table 1).

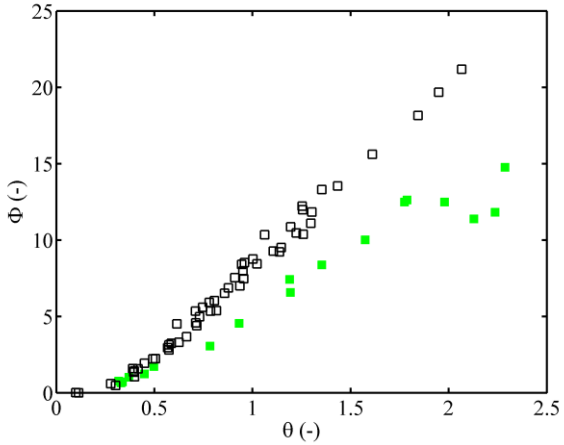

Fig. 7. Dimensionless sediment flow rate (Einstein parameter) versus dimensionless bed shear stress (bed Shields parameter). Legend: empty square – TLT50, full square – FA60.

One of the most important integral quantities is the sediment flow rate. In Figure 7, it is plotted against the bed Shields parameter, with which it closely correlates. According to Figure 7, the FA60 sediment grains are less

mobile than the TLT50-grains at high bed shear. The dimensionless numbers should take the different densities and sizes of the two granular fractions into account and the difference might be due to some other effect.

The results of the comparison of the fractions presented in Figures 8 and 9 Figure 8 seem to be in line with the result in Figure 7. The bed Froude number for FA60-flows is slightly smaller than for the TLT50-flow at the same bed Shields parameter. It is important to see that both fractions produce a maximum value of Fr at a certain value of Shields and that this threshold value of Shields is approximately the same for both fractions.

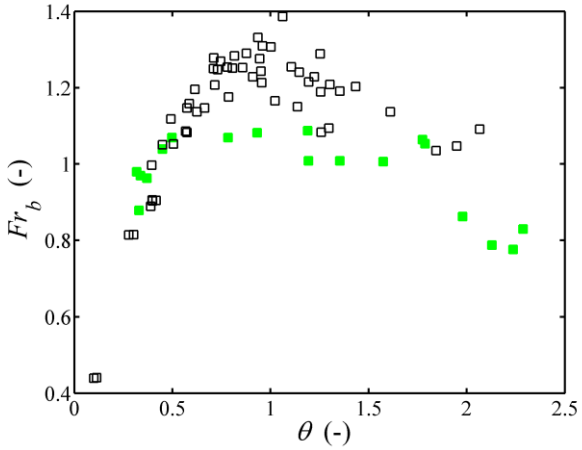

Fig. 8. Froude number dependent on shear stress, Legend: empty square – TLT50, full square – FA60.

The dimensionless equivalent roughness of the top of the FA60-deposit is higher than the roughness of the TLT50-deposit, see Figure 9. In both cases, there is a strong correlation between the dimensionless roughness and the bed Shields parameter. Apparently, the difference in the dimensionless roughness of the two fractions is associated with the fraction mobility and transport rate because the dimensionless roughness does not differ at low bed shear where the transport is weak and bed friction is dominated by bed surface friction.

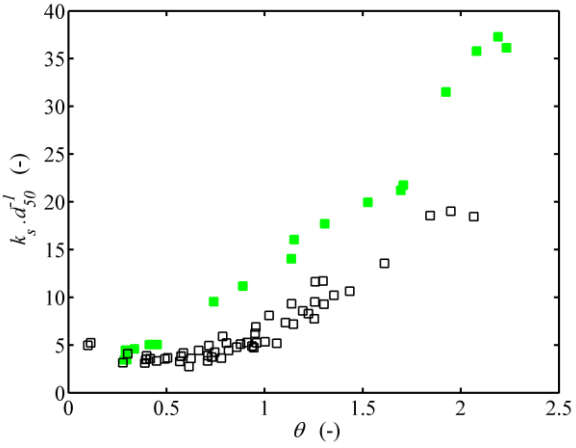

Fig. 9. Dimensionless bed roughness versus dimensionless bed shear stress, Legend: empty square – TLT50, full square – FA60.

4 Comparison of FA60-experiment with KT-based model prediction

Our bed-load transport predictive model based on classical kinetic theory proved to successfully predict the TLT50-flow [6] and the TLT25-flow [12]. The FA60-sediment laden flow is also collisional transport dominated and hence it is a natural candidate for modelling using the kinetic theory of granular flows. The model predicts the sediment transport rate and other flow quantities on the basis of considering flow conditions at layered flow interfaces.

4.1 Model assumptions and structure

The model employs constitutive equations of the classical kinetic theory and employ them to the bottom of the collisional part of the transport layer. The simplification of the extended kinetic theory (c tends to 1) is not applied to this interface because the local concentration is identified to vary at the interface (reaching low values of low bed shear stress and never reaching value near 1 at high bed shear) and also the testing of the extended kinetic theory on our experimental results did not show satisfactory results [13].

The model is described in details in [6]. It assumes simple linear distributions of concentration and velocity in the collisional part of the transport layer. The concentration is zero on the top of collisional layer and the velocity of particles in the dense layer is neglected. The local slip velocity between particles and water is neglected too. Also neglected is the diffusive term in the energy balance constitutive relation applied to the bottom of the collisional part of the transport layer.

Model predictions presented in the next paragraph are obtained for the following interfacial conditions: the inputs are the experimental thickness of the collisional layer (and hence the flow depth is predicted) and the experimental local concentration at the bottom of the collisional layer, c_d.

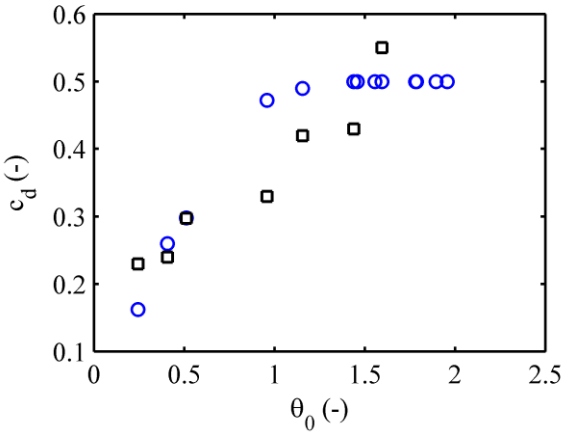

Fig. 10. Concentration at bottom of collisional layer versus dimensionless bed shear stress, Legend: blue circle – obtained from experiment using method [8], black square – obtained from experimental concentration distribution.

The interfacial concentration c_d is determined from experimental values of solids flow rate, interfacial velocity and thickness of the collisional layer using a method described in [8]. For the FA60 flow, such determined c_d can be compared with c_d values obtained from measured concentration distributions. The local concentration is selected at the position where the distribution exhibits a distinct abrupt change in local concentration as in Figures 3 and 4. This position differs slightly from the visually observed position of the bottom of the collisional layer in Figures 3 and 4, which can be attributed to uncertainty in visual observation of this interface. The c_d-values are compared in Figure 10 and a good agreement is found at low values of the dimensionless bed shear stress (predicted by the model, θ_0), where c_d tends to significantly vary with the bed Shields parameter.

The material constants of the model were set to the following values for the FA60-material: the coefficient of internal friction at the top of bed $\beta_0 = 0.6$, the bed concentration $c_0 = 0.6$, and the dry restitution coefficient, $\varepsilon = 0.58$.

4.2 Model predictions

The model predicts the thickness of the dense part of transport layer, y_d, which develops in the layered FA60 flow at high bed shear as observed in the experiment (see Figure 2). Figure 11 indicates that the model predicts the development of the layer well including its relation with the bed shear stress. It is also successful in predicting the incipient value of the bed shear stress at which the layer starts to develop. The worst agreement is at the highest θ_0 and the reason will be discussed later.

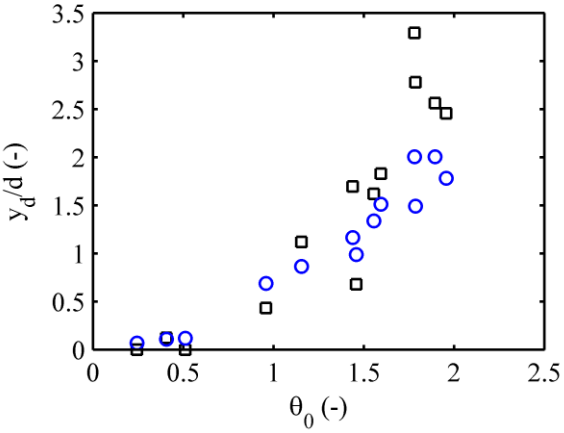

Fig. 11. Thickness of dense part of transport layer versus dimensionless bed shear stress for FA60 flow. Legend: black square – experiment, blue circle – model prediction.

The local velocity at the top of the transport layer, u_c, is another interfacial parameter predicted by the model. Again, the trend of increasing the velocity u_c, with increasing θ_0 is captured well in the model predictions and it is in a good agreement with the experimental results in Figure 12. The worst agreement is at the highest θ_0 subject to later discussion.

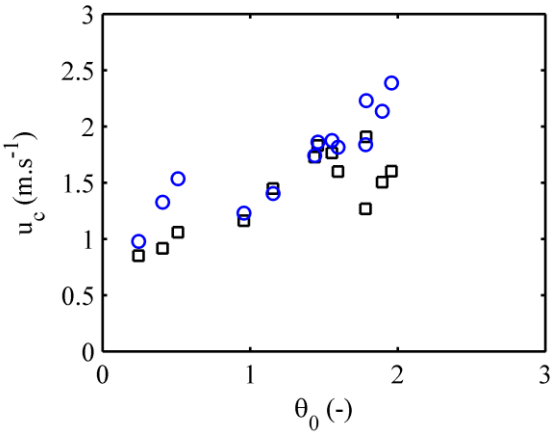

Fig. 12. Local velocity at top of transport layer versus dimensionless bed shear stress for FA60 flow. Legend: black square – experiment, blue circle – model prediction.

The results in Figure 12 are plotted in the parity plot of Figure 13 in order to quantify the difference between the measured and predicted values of u_c. It indicates that the worst predictions over-predict the local velocity with more than 25 per cent.

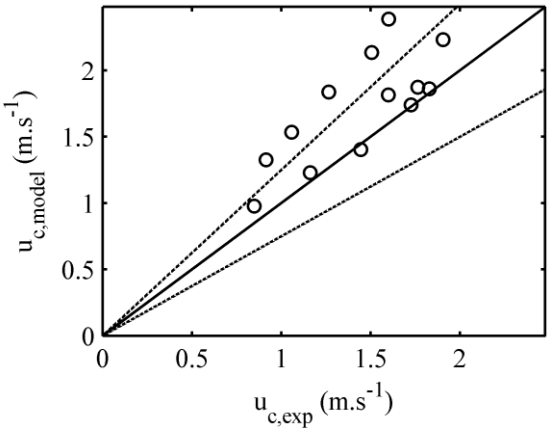

Fig. 13. Parity plot for experimental and predicted velocity at top of transport layer of FA60 flow. Legend: lines of perfect fit and of ± 25 per cent deviation.

As discussed in [6], the model can be applied in its standard predictive form considering the flow depth, H, as one of the model inputs (together with flow slope etc.) in order to produce thicknesses of individual layers and flow rates of solids and mixture as model outputs. Alternatively, it can use the thickness of the collisional part of the transport layer instead of the flow depth as one the model inputs and get the flow depth as one of the outputs. This alternative use of the model is suitable for comparing model predictions with experiments which give information about the thickness of the collisional layer. The flow depth predicted by the model is compared with the measured flows depths of FA60 flows in the parity plot of Figure 14.

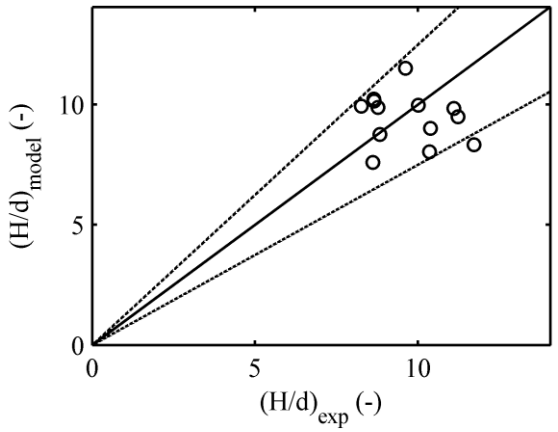

Fig. 14. Parity plot for predicted and experimental depth (normalized by grain size) of FA60 flow. Legend: lines of perfect fit and of ± 25 per cent deviation.

The discussed predictive model is a sediment transport model and hence the sediment flow rate, q_s, is its most important predicted quantity. Figure 15 shows that the prediction of is q_s good except for the highest measured flow rates of sediment, where the model tends to under-predict. The highest measured flow rates of sediment correspond with highest bed shear stresses and thus the weak prediction of q_s, corresponds with the weak predictions of y_d (Figure 11) and u_c (Figure 12) at the highest values of θ_0 ($\theta_0 > 1.5$ approximately). An analysis of a development of the transport layer showed that the top of the transport layer actually approaches the water surface and the concentration of at the top of the transport layer, c_c, is no longer zero ($c_c > 0$) if θ_0 is very high (see e.g. Figure 5). In the model, $c_c = 0$ is one of the assumptions and therefore the predictions of y_d, u_c, and q_s are affected by the fact that this assumption is no longer valid at $\theta_0 > 1.5$ for FA60 flows.

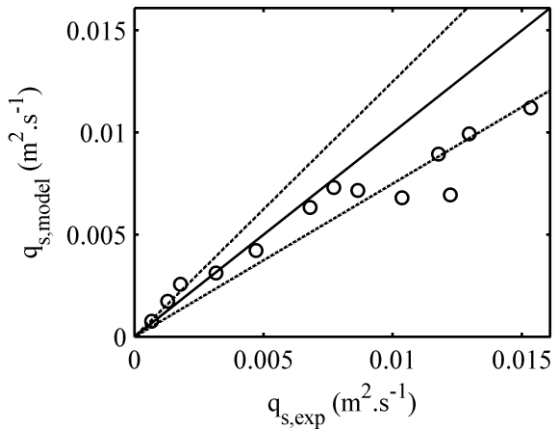

Fig. 15. Parity plot for experimental and predicted flow rate of sediment of FA60 flow. Legend: lines of perfect fit and of ± 25 per cent deviation.

5 Conclusions

Flow conditions at interfaces of layered flow transporting plastic FA60 grains in the upper plane bed regime were studied experimentally and predicted by our kinetic-theory based transport model. The analysis showed that

- the local concentration at the bottom of the collisional part of the transport layer tends to considerably vary with the bed shear stress provided that the transport layer does not become so thick that its top approaches the water surface;
- the velocity at the top of the transport layer and the thickness of the dense part of the transport layer vary with the bed shear stress and the predictive model captures this variation provided that the model assumptions are satisfied, namely the concentration at the top of the transport layer remains zero.

The transport model used its predictions of interfacial conditions to calculate the sediment flow rate by integrating simplified velocity and concentration distributions across the transport layer of the sediment-laden flow. For FA60 flow, the prediction is satisfactory in the range of the beds hear stresses where the predictions of the interfacial conditions are successful as well, i.e. for flows with bed Shields stress not exceeding say 1.5.

The research has been supported by the Czech Science Foundation through the grant project No. 16-21421S.

References

1. D. Berzi, ASCE J. Hydraul. Eng. **137**(10), 1200-1207 (2011)
2. H. Capart, L. Fraccarollo, Geophys. Res. Lett. 38. L20402 (2011)
3. D. Berzi, L. Fraccarollo, Geophys. Phys. Fluids **25**, 106601 (2013)
4. B. Spinewine, H. Capart, J. Fluid Mech. **731**, 579–613 (2013)
5. D. Berzi, L. Fraccarollo, Phys. Rev. Lett. **115**, 194501 (2015)
6. V. Matoušek, Š. Zrostlík, *River Flow 2018* (IAHR, Lyon, 2018)
7. V. Matoušek, V. Bareš, J. Krupička, T. Picek, Š. Zrostlík, Can. J. Chem. Eng. **94**, 1076-1083 (2016)
8. V. Matoušek, V. Bareš, J. Krupička, T. Picek, Š. Zrostlík, *River Flow 2016* (IAHR, Saint Louis, 2016)
9. V. Matoušek, V. Bareš, J. Krupička, T. Picek, Š. Zrostlík, J. Hydrol. Hydromech. **63**(4), 318-326 (2015)
10. B. Spinewine, H. Capart, L. Fraccarollo, M. Larcher, Exp. Fluids **50**(6), 1507–1525 (2011)
11. J. Krupička, T. Picek, Š. Zrostlík, Acta Polytech. **58**(3), 171-178 (2018)
12. V. Matoušek, *Conveying and Handling of Particulate Solids 2018* (London, 2018)
13. V. Matoušek, Š. Zrostlík, J. Hydrol. Hydromech. **66**(3), 330-336 (2018)